# CHARACTERIZATION OF AN ADAPTIVE TECHNIQUE TO REDUCE COMBUSTION THERMOCHEMISTRY

**Americo Barbosa da Cunha Junior**
**Luís Fernando Figueira da Silva**
Departamento de Engenharia Mecânica
Pontifícia Universidade Católica do Rio de Janeiro
Rua Marquês de São Vicente, 225, Gávea, Rio de Janeiro - RJ, Brasil - 22453-900
americo.cunhajr@gmail.com — luisfer@esp.puc-rio.br

***Abstract.***
*The study of combustion requires the description of the thermochemistry of elementary reactions. Modern detailed chemical kinetic description of hydrocarbon mixtures combustion with air involves tens of species and hundreds of elementary reactions. Since each of these elementary reactions evolve at timescales which may span over several orders of magnitudes, the resulting model is inherently stiff. These characteristics imply that the numerical integration of the detailed thermochemical evolution equations is the most expensive task when a detailed description of combustion chemistry is sought, for instance, in computational fluid dynamics models. This work presents a technique, dubbed in situ adaptive tabulation (ISAT), which has been implemented in order to reduce the integration time of the system of equations governing the thermochemical evolution of reactive mixtures. The technique is tested in a modification of the classical Partially Premixed Reactor (PaSR) called Pairwise Mixing Stirred Reactor (PMSR) and the results obtained characterize the efficiency of the algorithm, demonstrating a reduction of up to* 46% *in computational time when compared to the direct integration of the governing equations.*

***Keywords:*** *combustion modelling, thermochemistry reduction, adaptive tabulation*

## 1. INTRODUCTION

Computational models to predict the behavior of an industrial device that uses combustion on its operation may require the solution of partial differential equations that represent the balance of mass, momentum, chemical species and energy. These models may include a detailed kinetic mechanism for the description of the physicochemical phenomena involved. Typically, such reaction mechanisms for mixtures of hydrocarbons with air involve tenths of species, hundreds of elementary reactions and timescales that vary up to nine orders of magnitude Williams (1985).

The challenge numerical simulation of these models, is related to the reaction rate of chemical species, which is difficult to model and imposes stiffness to system, since it has a nonlinear nature and presents a strong dependence with the size of the reaction mechanism. Therefore, the numerical solution of a detailed reaction mechanism is computationally demanding, which justifies the development of techniques that allow for the reduction of the computational cost associated.

This work presents a technique, dubbed *in situ* adaptive tabulation (ISAT), Pope (1997), which has been implemented in order to reduce the integration time of the system of equations governing the evolution of reactive mixtures. The methodology consists in progressively creating a table which stores solutions and initial conditions for the system of governing equations. A search is performed along this table whenever the integration of these equations is required and a tabulated solution is recovered. If the information recovered from the table is satisfactory, in a sense implicit to the technique, a linear extrapolation gives an adequate approximate solution. This approximate solution has a local error which is second order accurate in time, thus ensuring that the global error is of first order. A characterization of this technique is presented which details benefits and the shortcomings of this technique when applied to simple and complex reactive systems.

## 2. MATHEMATICAL FORMULATION

In this section the mathematical formulation of the problem is briefly described, further details may be found in Pope (1997) or Cunha Jr (2010).

### 2.1 The Geometry of Reactive Systems

To study a reduction technique for combustion thermochemistry is desirable to consider a physical system in which the behavior depends primarily on the processes of transport and reaction of the chemical species. Thus,

consider a transient spatially homogeneous reactive mixture evolving adiabatically and at constant pressure in a continuous flow reactor. The thermodynamical state of a fluid particle in the reactor may be completely determined by the mass fraction $Y_i$ $(i = 1, \cdots, n_s)$ of the $n_s$ chemical species, the specific enthalpy $h$ and pressure $p$, which can be lumped in the *composition* vector defined as

$$\boldsymbol{\phi} \equiv (h, p, Y_1, \cdots, Y_{n_s})^{\mathsf{T}}, \tag{1}$$

where the superscript $^{\mathsf{T}}$ denotes the transposition operation. One should note that, due to the invariance of the system number of atoms, which ensures the total conservation of the mass, the components of vector $\boldsymbol{\phi}$ are not linearly independent.

In the framework of the transported probability density function (PDF) models Pope (1985), a reactive system may be described by an ensemble $(j)$ of stochastic particles, which mimic the behavior of the fluid system.

The evolution of the composition of each particle in a reactor can be written in a general framework according to the following set of ordinary differential equations

$$\frac{d\boldsymbol{\phi}^{(j)}}{dt} = -\boldsymbol{\Gamma}^{(j)}(t) + \boldsymbol{S}(\boldsymbol{\phi}^{(j)}, t), \tag{2}$$

where $\boldsymbol{\Gamma}^{(j)}(t)$ is the rate of change due to mixing and $\boldsymbol{S}(\boldsymbol{\phi}^{(j)}, t)$ is the rate of change associated to the chemical reactions. One may integrate Eq.(2) from an initial time $t_0$ to a time $t$

$$\boldsymbol{\phi}^{(j)}(t) = \boldsymbol{\phi}_0^{(j)} - \int_{t_0}^{t} \boldsymbol{\Gamma}^{(j)}(t')dt' + \int_{t_0}^{t} \boldsymbol{S}(\boldsymbol{\phi}^{(j)}, t')dt', \tag{3}$$

and define the *reaction mapping*

$$\boldsymbol{R}(\boldsymbol{\phi}_0^{(j)}, t) \equiv \boldsymbol{\phi}^{(j)}(t), \tag{4}$$

as the solution of Eq.(2) after a time $t$ starting from the initial composition $\boldsymbol{\phi}^{(j)}(t_0) = \boldsymbol{\phi}_0^{(j)}$. The reaction mapping corresponds to a trajectory in *composition space*, which, for large values of $t$, tends to the equilibrium composition for the given enthalpy and pressure on $\boldsymbol{\phi}_0^{(j)}$. The composition space is the $(n_s + 2)$–dimensional Euclidean space where where the first direction is associated with the enthalpy, the second with the pressure and the other $n_s$ are related to the chemical species.

### 2.2 Pairwise Mixing Stirred Reactor

The classical *Partially Stirred Reactor* (PaSR), used by Correa (1993), describes $\boldsymbol{\Gamma}(t)$ by the interaction by exchange with the mean (IEM) micromixing model but, for the purpose of testing a thermochemistry reduction technique, it is desirable to employ a mixing model that leads to a composition region accessed during the solution process which is "wider" than that provided by the IEM model. A modified version of PaSR model called *Pairwise Mixing Stirred Reactor* (PMSR), Pope (1997), is designed to yield a much larger accessed region, and, hence, should provide a stringent test to the ability of ISAT technique to yield a reduction in computational time.

In the PMSR model the reactor consists of an even number $n_p$ of particles, initially arranged in pairs $(j_1, j_2)$ such that the particles $(1, 2)$, $(3, 4)$, $\cdots$, $(n_p - 1, n_p)$ are partners. Given a time step, $\Delta t$, for each discrete times $k\Delta t$, where $k$ is an integer, the model is characterized by three types of events: *inflow*, *outflow* and *pairing*. The inflow and outflow events consist of randomly selecting $n_{in} \equiv ceil\,(0.5\Delta t/\tau_r n_p)$ pairs of particles, being $\tau_r$ the residence time within the reactor, and exchanging the thermodynamical properties by the properties of a prescribed inflow. The pairing event consists of randomly selecting for pairing a number of pairs of particles, different from the inflow particles, equal to $n_{pair} \equiv ceil\,(0.5\Delta t/\tau_p n_p)$, being $\tau_p$ the pairwise time. Then the chosen particles (inflow/outflow and paring) are randomly shuffled. Between these discrete times, the pairs of particles $(j_1, j_2)$ evolve according to the following mixing law

$$\frac{d\boldsymbol{\phi}^{(j_1)}}{dt} = -\frac{\boldsymbol{\phi}^{(j_1)} - \boldsymbol{\phi}^{(j_2)}}{\tau_m} + \boldsymbol{S}(\boldsymbol{\phi}^{(j_1)}, t), \tag{5}$$

$$\frac{d\boldsymbol{\phi}^{(j_2)}}{dt} = -\frac{\boldsymbol{\phi}^{(j_2)} - \boldsymbol{\phi}^{(j_1)}}{\tau_m} + \boldsymbol{S}(\boldsymbol{\phi}^{(j_2)}, t). \tag{6}$$

### 2.3 Numerical Integration

An operator splitting technique Yang and Pope (1998) is employed to solve Eq.(2). The overall process of integration via operator splitting technique can be represented as

$$\boldsymbol{\phi}^{(j)}(t) \overset{mixing}{\longrightarrow} \boldsymbol{\phi}^{(j)}_{mix}(t+\Delta t) \overset{reaction}{\longrightarrow} \boldsymbol{\phi}^{(j)}(t+\Delta t), \tag{7}$$

where given an initial composition $\boldsymbol{\phi}^{(j)}_0$ and a time step $\Delta t$, the first fractional step integrates the pure mixing system,

$$\frac{d\boldsymbol{\phi}^{(j)}}{dt} = -\boldsymbol{\Gamma}^{(j)}(t), \tag{8}$$

to obtain $\boldsymbol{\phi}^{(j)}_{mix}(t+\Delta t)$. Then, the pure chemical reaction system,

$$\frac{d\boldsymbol{\phi}^{(j)}}{dt} = \boldsymbol{S}(\boldsymbol{\phi}^{(j)}, t). \tag{9}$$

is solved from an initial composition $\boldsymbol{\phi}^{(j)}_{mix}(t+\Delta t)$ over a time step $\Delta t$ and gives $\boldsymbol{\phi}^{(j)}(t+\Delta t)$.

The operator splitting technique allows to solve each term in the evolution equation, Eq.(2), separately, using specific efficient numerical methods to treat the particular features inherent to the physical phenomenon modeled by each term Fox (2003).

### 2.4 Linearized Reaction Mapping

Consider a composition $\boldsymbol{\phi}$[1] and an *initial composition* $\boldsymbol{\phi}_0$, so that the series expansion of the reaction mapping of the composition around the initial one is

$$\boldsymbol{R}(\boldsymbol{\phi}, t) = \boldsymbol{R}(\boldsymbol{\phi}_0, t) + \boldsymbol{A}(\boldsymbol{\phi}_0, t)\delta\boldsymbol{\phi} + \mathcal{O}(||\delta\boldsymbol{\phi}||^2), \tag{10}$$

where $\delta\boldsymbol{\phi} \equiv \boldsymbol{\phi} - \boldsymbol{\phi}_0$, the *mapping gradient matrix* is the $n_\phi \times n_\phi$ matrix $\boldsymbol{A}(\boldsymbol{\phi}_0, t)$ with components given by

$$A_{ij}(\boldsymbol{\phi}_0, t) \equiv \frac{\partial R_i}{\partial \phi_{0_j}}(\boldsymbol{\phi}_0, t), \tag{11}$$

the $\mathcal{O}(||\delta\boldsymbol{\phi}||^2)$ denotes terms that have order $||\delta\boldsymbol{\phi}||^2$ and $||\cdot||$ denotes the Euclidean norm of a vector.

The *linear approximation* $\boldsymbol{R}^l(\boldsymbol{\phi}, t)$ is obtained by neglecting the high order terms of Eq.(10) and is second order accurate at a connected region of composition space centered at $\boldsymbol{\phi}_0$. The shape of this region is unknown before the calculations, but the ISAT algorithm approximates this region by a hyper-ellipsoid, as will be shown in section 2.5 The *local error* of this linear approximation is defined as the Euclidean norm of the difference between the reaction mapping at $\boldsymbol{\phi}$ and the linear approximation for it around $\boldsymbol{\phi}_0$,

$$\varepsilon \equiv ||\boldsymbol{R}(\boldsymbol{\phi}, t) - \boldsymbol{R}^l(\boldsymbol{\phi}, t)||. \tag{12}$$

### 2.5 Ellipsoid of Accuracy

The accuracy of the linear approximation at $\boldsymbol{\phi}_0$ is controlled only if the local error is smaller than a positive *error tolerance* $\varepsilon_{tol}$, which is heuristically chosen. The *region of accuracy* is defined as the connected region of the composition space centered at $\boldsymbol{\phi}_0$ where local error is not greater than $\varepsilon_{tol}$. As shown in Pope (1997), this

[1] From now on the superscript $^{(j)}$ is omitted for the sake of notation simplicity.

region is approximated by a hyper-ellipsoid centered at $\boldsymbol{\phi}_0$ which is dubbed *ellipsoid of accuracy* (EOA), and is mathematically represented by the following equation

$$\delta\boldsymbol{\phi}^{\mathrm{T}}\boldsymbol{L}\boldsymbol{L}^{\mathrm{T}}\delta\boldsymbol{\phi} \leq \varepsilon_{tol}^2, \tag{13}$$

where the EOA Cholesky matrix $\boldsymbol{L}$ is lower triangular, Golub and Van Loan (1996).

The adaptive step of ISAT algorithm involves the solution of the following geometric problem: given a hyper-ellipsoid centered at $\boldsymbol{\phi}_0$ and a *query composition*, $\boldsymbol{\phi}_q$, outside it, determine a new hyper-ellipsoid of minimum hyper-volume, centered at $\boldsymbol{\phi}_0$, which encloses both the original hyper-ellipsoid and the point $\boldsymbol{\phi}_q$. The solution of this problem is presented by Pope (2008) and is not shown here for sake of brevity.

### 2.6 *In Situ* Adaptive Tabulation

Initially the ISAT algorithm receives the time step $\Delta t$ and the tolerance $\varepsilon_{tol}$. Then, in every time step, the ISAT algorithm receives a query composition $\boldsymbol{\phi}_q$ and returns an approximation for the corresponding reaction mapping $\boldsymbol{R}(\boldsymbol{\phi}_q, t)$. This approximation is obtained via numerical integration of Eq.(9) or by the linear approximation $\boldsymbol{R}^l(\boldsymbol{\phi}_q, t)$.

During the reactive flow calculation, the computed values are sequentially stored in a table for future use. This process is known as *in situ* tabulation. The ISAT table, which is created by the tabulation process, includes the initial composition $\boldsymbol{\phi}_0$, the reaction mapping $\boldsymbol{R}(\boldsymbol{\phi}_0, t)$ and the mapping gradient matrix $\boldsymbol{A}(\boldsymbol{\phi}_0, t)$. Using these elements it is possible to construct the linear approximation. As the calculation proceeds, a new query composition, $\boldsymbol{\phi}_q$, is received by ISAT, the table is transversed until a $\boldsymbol{\phi}_0$ is found that is close to $\boldsymbol{\phi}_q$. Depending on the accuracy, the linear approximation around $\boldsymbol{\phi}_0$ is returned or the reaction mapping of $\boldsymbol{\phi}_q$ is obtained by direct integration of Eq.(9).

The ISAT table is a binary search tree, since this data structure allows for searching an information in $\mathcal{O}(\log_2 n_{tab})$ operations, where $n_{tab}$ is the total number entries in the tree, if the tree is balanced Knuth (1998). The binary search tree is basically formed by two types of elements, nodes and leaves. Each leaf of the tree stores the following data:

- $\boldsymbol{\phi}_0$: initial composition;
- $\boldsymbol{R}(\boldsymbol{\phi}_0, t)$: reaction mapping at $\boldsymbol{\phi}_0$;
- $\boldsymbol{A}(\boldsymbol{\phi}_0, t)$: mapping gradient matrix at $\boldsymbol{\phi}_0$;
- $\boldsymbol{L}$: EOA Cholesky matrix.

Each node of the binary search tree has an associated *cutting plane*. This plane is defined by a *normal vector*

$$\boldsymbol{v} \equiv \boldsymbol{\phi}_q - \boldsymbol{\phi}_0, \tag{14}$$

and a scalar

$$a \equiv \boldsymbol{v}^{\mathrm{T}}\left(\frac{\boldsymbol{\phi}_q + \boldsymbol{\phi}_0}{2}\right), \tag{15}$$

such that all composition $\boldsymbol{\phi}$ with $\boldsymbol{v}^T\boldsymbol{\phi} > a$ are located to the right of the cutting plane, all other compositions are on the left, as sketched in Figure 1. The cutting plane construction defines a search criterion in the binary search tree.

If, during the calculation, a query point $\boldsymbol{\phi}_q$ is encountered that is within the region of accuracy, i.e. $\varepsilon \leq \varepsilon_{tol}$, but outside the estimate of EOA, then the EOA growth proceeds as detailed in Pope (2008). The first three items stored in the binary search tree leaf [$\boldsymbol{\phi}_0$, $\boldsymbol{R}(\boldsymbol{\phi}_0, t)$ *and* $\boldsymbol{A}(\boldsymbol{\phi}_0, t)$] are computed once, whereas $\boldsymbol{L}$ changes whenever the EOA is grown.

Once a query composition $\boldsymbol{\phi}_q$ is received by the ISAT table, the binary search tree is initialized as a single leaf ($\boldsymbol{\phi}_0 = \boldsymbol{\phi}_q$) and the exact value of the reaction mapping is returned.

The subsequent steps are:

1. Given a query composition the tree is transversed until a leaf ($\boldsymbol{\phi}_0$) is found.
2. Equation (13) is used to determine if $\boldsymbol{\phi}_q$ is inside EOA or not.

3. If $\boldsymbol{\phi}_q$ is inside EOA, the reaction mapping is given by the linear approximation. This is the first of four outcomes, called *retrieve*.

4. If $\boldsymbol{\phi}_q$ is outside EOA, direct integration is used to compute the reaction mapping, and the local error is measured by Eq.(12).

5. If the local error is smaller than tolerance, $\varepsilon_{tol}$, the EOA is grown according to the procedure presented in Pope (2008) and the reaction mapping is returned. This outcome is called *growth*.

6. If local error is greater than the tolerance $\varepsilon_{tol}$ and the maximum number of entries in the binary search tree is not reached, a new record is stored in the binary search tree based on $\boldsymbol{\phi}_q$ and the reaction mapping is returned. The original leaf is replaced by a node with the left leaf representing the old composition $\boldsymbol{\phi}_0$ and the right leaf the new one $\boldsymbol{\phi}_q$ as shown in Figure 2. This outcome is an *addition*.

7. If the local error is greater than the tolerance $\varepsilon_{tol}$ and the maximum number of entries in the binary search tree is reacted, the reaction mapping is returned. This outcome is called *direct evaluation*.

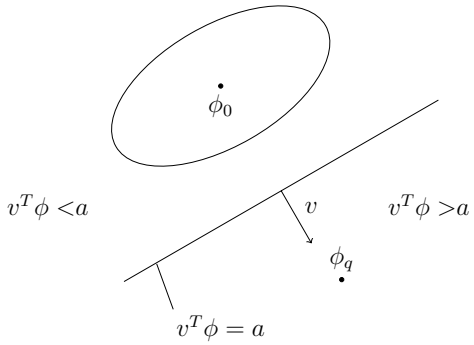


Figure 1. Cutting plane in relation to EOA position.

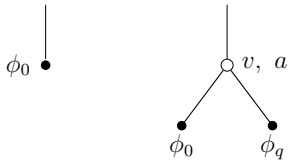


Figure 2. Binary search tree before and after the addition of a new node.

## 3. RESULTS AND DISCUSSION

In order to assess the accuracy and the performance of the ISAT technique implementation, this section presents benchmark tests which compare the calculation results obtained by the ISAT technique with those issued from the direct integration (DI) of the evolution equations in a PMSR.

### 3.1 Analysis of the ISAT Accuracy

The considered PMSR is initially filled with a fuel-lean (equivalence ratio = 0.7) mixture of $CO/O_2$ at 2948.5 K and 1 atm. The reaction of $CO$ with $O_2$ involves 4 species and 3 reactions, Gardiner (2000). At every time step, a fuel-lean (equivalence ratio = 0.7) mixture of $CO/O_2$ enters the reactor at 300 K and 1 atm. The constant pressure and enthalpy equilibrium state associated to the inflow mixture is reached at 2948.5 K. Two time scales situations are studied for this PMSR, which are presented in Table 1. For the first one, which defines the first test case, $\tau_m/\tau_r = \tau_p/\tau_r = 1/2$, so that the pairwise/mixing time scales are of the same order of magnitude as the residence time, thus allowing to obtain partially stirred reactor (PaSR) conditions. For the second test case, which is defined by the second configuration of time scales presented in the Table 1, $\tau_m/\tau_r = \tau_p/\tau_r = 1/10$, so that the pairwise/mixing time scales are small when compared to the residence time. Thus, the reactor should behave almost as a perfect stirred reactor (PSR), where the processes of mixing and pairing occur instantaneously. This study uses a binary search tree with a maximum of $50,000$ entries; time step of $\Delta t = 10\ \mu$s; solver relative tolerance of $\varepsilon_{rel} = 10^{-6}$; solver absolute tolerance of $\varepsilon_{abs} = 10^{-9}$ and ISAT error tolerance of $\varepsilon_{tol} = 10^{-3}$.

Table 1. Parameters used in the simulation of a $CO/O_2$ mixture in a PMSR.

| | | Case 1 | Case 2 |
|---|---|---|---|
| number of particles | $N$ | 1024 | 1024 |
| residence time ($\mu$s) | $\tau_r$ | 200 | 1000 |
| mixing time ($\mu$s) | $\tau_m$ | 100 | 100 |
| pairwise time ($\mu$s) | $\tau_p$ | 100 | 100 |

Figure 3 shows the comparison between DI and ISAT computational results for the ensemble average of the reduced temperature $\langle T \rangle^*$ in both cases, where the ensemble average operator is defined as

$$\langle \psi \rangle \equiv \frac{1}{n_p} \sum_{j=1}^{n_p} \psi^{(j)}, \tag{16}$$

being $\psi$ a generic property of the reactive system. For the result of case 1, which spans over a range of 500 residence times, one can observe good qualitative agreement. The ensemble average value rapidly increases from the initial value, then decreases to reach the statistically steady state regime around $\langle T \rangle^* = 0.35$. The analysis of this figure shows that the statistically steady state regime is reached after 10 residence times. In case 2, where a range of 250 residence times is computed, one can also observe a good qualitative agreement for the ensemble average of reduced temperature. Again, the overall history of the PMSR is the same for DI and ISAT. Similar results, not shown here, were obtained for the other thermochemical properties of the reactors.

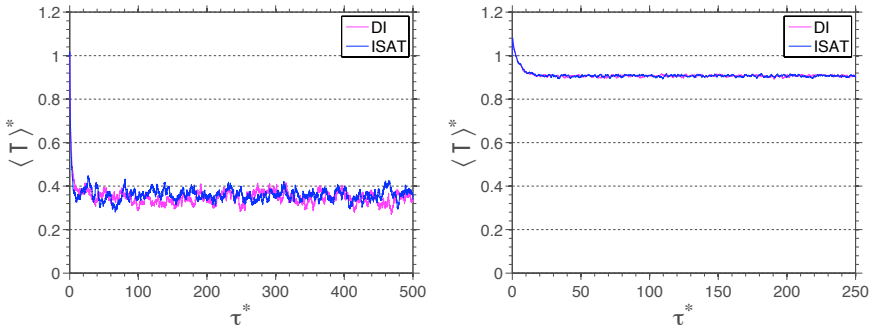


(a) Evolution of $\langle T \rangle^*$ for case 1. (b) Evolution of $\langle T \rangle^*$ for case 2.

Figure 3. Comparison between DI and ISAT results of ensemble average reduced temperature.

Aiming to quantify the discrepancies between the values obtained via DI and ISAT, Figure 4 presents the evolution of the relative local error of the ensemble average reduced temperature, denoted by $\varepsilon_{r,\langle T \rangle^*}$. The relative local error is defined as the absolute value of the difference between DI and ISAT results over DI results. Concerning the errors in case 1 one can observe a large statistical variation due to stochastic nature of the PMSR model, with amplitudes reaching 40%. In case 2, relative errors of the order of 1% only can be observed.

The difference among cases is due to the behavior of each reactor at the statistically steady state regime. Indeed, the behavior of the reactor of case 2 is governed by a competition between the chemical and residence times only, therefore the thermodynamical properties steady state probability density function is spread over a smaller range than in case 1, where the mixing and pairing time scales are large. This behavior is illustrated in Figure 5, which presents the comparison between DI and ISAT computations of the mean PDF, averaged over the last 50 residence times, of the reduced temperature for cases 1 and 2. This figure underscores the influence of the controlling parameters of the PMSR, i.e., the time scales ratios, on the thermochemical conditions prevailing within each reactor. Indeed, the temperature within the reactor of case 2 is such that almost only burned gases are found. On the other hand, case 1 reactor is characterized by a bimodal temperature distribution with a large probability of finding $T^* = 0.1$ and a broader temperature distribution leaning to the burned gases.

In the early development of the ISAT technique Pope (1997) it was noted that the choice of the tolerance could affect the accuracy of the problem solution. In order to investigate the effect of the tolerance on the present results, Figure 6 presents the relative global error $\varepsilon_g$, as a function of the ISAT error tolerance for test

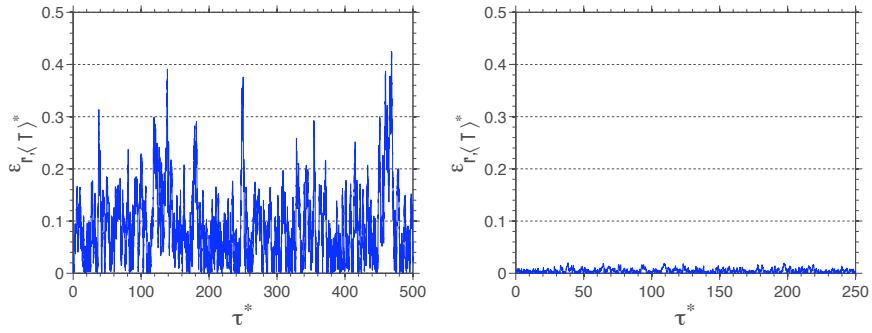


(a) Evolution of $\varepsilon_{r,\langle T\rangle^*}$ for case 1 (b) Evolution of $\varepsilon_{r,\langle T\rangle^*}$ for case 2

Figure 4. Evolution of relative local error of ensemble average reduced temperature.

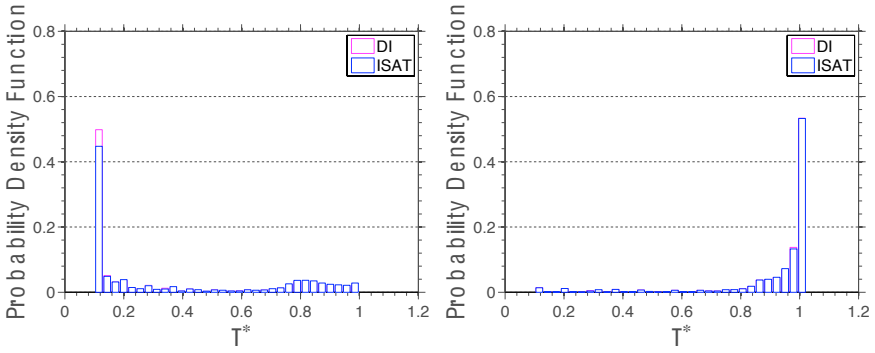


(a) PDF of $T^*$ for case 1. (b) PDF of $T^*$ for case 2.

Figure 5. Comparison between DI and ISAT computations of the mean histograms of the reduced temperature.

cases 1 and 2. The relative global error is over a time interval $\Delta\tau$ is defined as

$$\varepsilon_g \equiv \frac{1}{\Delta\tau}\int_t^{t+\Delta\tau} \frac{||\langle\boldsymbol{\phi}\rangle(t')_{DI} - \langle\boldsymbol{\phi}\rangle(t')_{ISAT}||}{||\langle\boldsymbol{\phi}\rangle(t')_{DI}||}dt', \tag{17}$$

where $\langle\boldsymbol{\phi}\rangle$ denotes the ensemble average vector and the subscripts $_{DI}$ and $_{ISAT}$ denote DI and ISAT calculations, respectively.

In both cases it is observed that the relative global error varies as the ISAT error tolerance is changed, reaching maximum and minimum values at $\varepsilon_{tol} = 10^{-3}$ and $\varepsilon_{tol} = 10^{-2}$ for case 1, and, $\varepsilon_{tol} = 10^{-2}$ and $\varepsilon_{tol} = 10^{-5}$ for case 2, respectively. From the analysis of the error metrics it is possible to characterize an ISAT table with 50k entries as one with a good qualitative reproduction of the results, accurate from a global point of view, but with low accuracy if the local properties are analyzed.

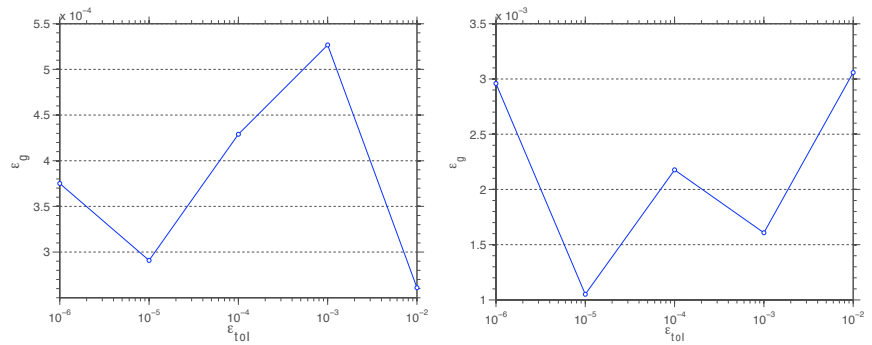


(a) $\varepsilon_g$ vs $\varepsilon_{tol}$ for case 1. (b) $\varepsilon_g$ vs $\varepsilon_{tol}$ for case 2.

Figure 6. Relative global errors as function of the error tolerance, using a binary search tree with 50k entries.

### 3.2 Analysis of the ISAT Performance

The comparison of evolution of the ISAT algorithm outputs and of the height of ISAT binary search tree as well as the corresponding rates of change, for cases 1 and 2, which parameters are given in Table 1, is presented in Figures 7 and 8. A first important observation is that the number of additions in both cases reaches the maximum allowed value in the binary search tree of 50k. As a consequence of the saturation of binary search tree, the additions curve reaches a steady state after 5.4 and 1.2 residence times in the first and second cases respectively. Note that these residence times correspond to 108 and 123 PMSR events (see section 2.2), which indicates that the ISAT table was saturated earlier when mixing is slow.

Figures 7 and 8 also show the evolution of the height of binary tree, which reaches steady state after 36 PMSR events (1.8 time of residence) in the first case and 76 PMSR events (0.4 time of residence) in the second case. It is also noteworthy that, in both cases, the tree height is an order of magnitude smaller than the total number of entries in the tree ($\sim$ 17k in case 1 and $\sim$ 7k in case 2). This difference between height and total entries in the tree ensures the efficiency of the process of searching for a new query, which may be performed up to three and seven times faster in cases 1 and 2, respectively, than a vector search.

In the first case, Figures 7 and 8 show that the number of growths presents a sharp rate of change around 1 residence time whereas, in the second case, this occurs around 5 residence times. In both cases, growth steady state occurs after 10 residence times. During both simulations the number of growths is always smaller than the process of additions. This indicates that the desirable massive increase of the ellipsoids of accuracy to form a better estimate for the region of accuracy is not observed. This behavior might circumstantial to the reaction mechanism of the carbon monoxide, since due to its simplicity (only 3 reactions) a small part of the realizable region should be assessed by the calculation.

Figures 7 shows that, after tree saturation occurs, the number of retrieves and direct evaluations exceed the number of additions in both cases. In case 1 there is a higher occurrence of the retrieve event, whereas in case 2 direct evaluation prevails. The number of retrieves exhibits a linear limit behavior in both cases. The ISAT behavior for the second case reflects the fact that the binary tree of this case is poor, i.e., contains too few compositions in the region accessed by the calculation. As a consequence, the number of direct evaluations vastly outnumbers the ISAT operations.

A sufficient condition for a calculation using the ISAT algorithm to be faster than the same calculation using DI is that the number of recoveries exceed the number of additions by a certain factor, which depends on the specific time of each output. From Figure 7 it is possible estimate these factors as greater than or equal to 100 and 5 for cases 1 and 2, respectively. Further details may be found at Cunha Jr (2010).

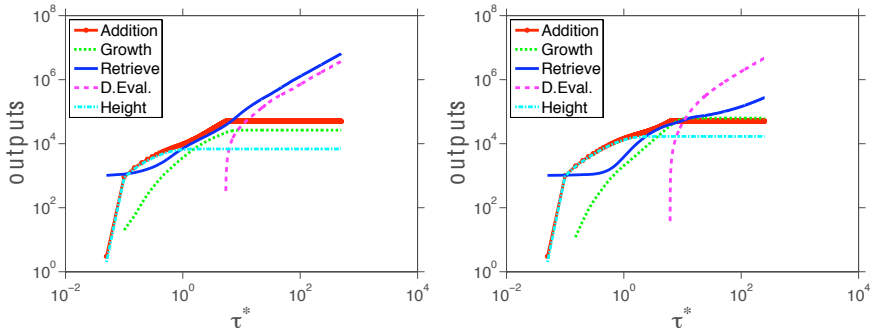


(a) Case 1. (b) Case 2.

Figure 7. Evolution of ISAT algorithm outputs and of the height of ISAT binary search tree.

As can be seen in Table 2, where a comparison of computational time is shown, cases 1 and 2, for $\varepsilon_{tol} = 10^{-3}$ are computed using DI in 4.330 ks and 3.051 ks respectively whereas, with the use of ISAT, the same cases spent 2.348 ks and 2.113 ks, respectively. Speed-up factors of 2.3 (case 1) and 1.4 (case 2) are obtained, where the speed-up factor is defined as the ratio between the computational time spent by DI and the computational time spent by ISAT. This table also allows to compare the computational time spent by DI and ISAT for different values of error tolerance. An increase in processing time is obtained as ISAT error tolerance is reduced, which is to be expected, given the fact that lower values of $\varepsilon_{tol}$ correspond to a smaller region of accuracy. Indeed, as $\varepsilon_{tol}$ is decreased, it is less likely that ISAT returns a retrieve, which is the ISAT output with lower computational cost. Clearly, in all cases the ISAT algorithm offers an advantage in terms of processing time, when compared to the process of direct integration, reducing on average the processing time in 46% for case 1 and in 31% for case 2.

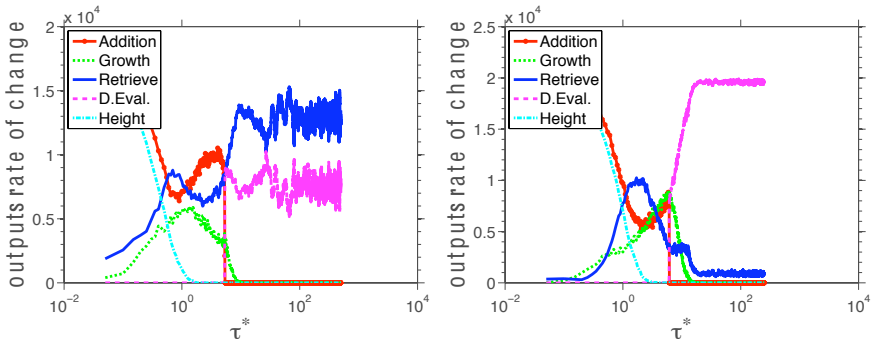


(a) Case 1. (b) Case 2.

Figure 8. Evolution of the rates of change of each ISAT algorithm outputs and of the height of ISAT binary search tree.

Table 2. Comparison between the computational time spent by DI and ISAT in cases 1 and 2 and the corresponding speed-up factors.

| | Case 1 | | Case 2 | |
|---|---|---|---|---|
| $\varepsilon_{tol}$ | time spent (ks) | speed-up | time spent (ks) | speed-up |
| DI | 4.3 | | 3.1 | |
| $10^{-2}$ | 1.9 | 2.3 | 2.1 | 1.5 |
| $10^{-3}$ | 2.3 | 1.9 | 2.1 | 1.5 |
| $10^{-4}$ | 2.4 | 1.8 | 2.1 | 1.5 |
| $10^{-5}$ | 2.5 | 1.7 | 2.2 | 1.4 |
| $10^{-6}$ | 2.6 | 1.7 | 2.2 | 1.4 |

### 3.3 Analysis of ISAT Memory Usage

Cases 1 and 2 previously studied are both modeled by a reaction mechanism with 4 species and use a binary search tree with 50,000 entries for ISAT simulations. These parameters lead to a memory consumption by the ISAT algorithm of approximately 40 Mbytes, which is very small when compared to the available in the used computers. However, if the number of species in reaction mechanism increases, say 52 as in typical methane/air mechanisms, the memory storage cost growths, as shown in Cunha Jr (2010). Indeed, a simulation of PMSR filled with a methane/air mixture and using a binary search tree with 60,000 entries uses approximately 3.2 Gbytes. This huge expense of memory is perhaps the greatest weakness of the ISAT algorithm. Note that no attempt was made to optimize the code performance.

## 4. FINAL REMARKS

This work presented ISAT technique as an option to evaluate the system of governing equations in a computational model with detailed combustion thermochemistry. The technique is assessed for its accuracy, performance, and memory usage in the numerical simulation of PMSR filled with carbon monoxide/oxygen mixture.

The ISAT technique shows good accuracy from a global point of view, with the relative global error smaller than 0.35% for all the reactor configurations tested. Concerning the error from a local point of view, ISAT technique was characterized by values of the maximum error of the mean properties within the reactor of up to 41%, which could be unacceptable depending on the application.

In terms of performance, the ISAT algorithm allows to reduce the computational time of the simulations in all cases tested, achieving speed-up factors of 2.3 (case 1) and 1.4 (case 2).

Regarding the memory usage, the ISAT technique is very demanding. In the simulation of the methane/air mixture using a binary search tree with 60,000 entries, not shown here, the algorithm required 3.2 Gbytes. Thus, based on this test case, this work underscores the memory usage as the major drawback of the ISAT algorithm.

An extension of this work would be the coupling of a detailed thermochemistry mechanism, using the ISAT technique, with the hybrid LES/PDF model by Andrade (2009) and Andrade et al. (2009) for description of

turbulent combustion. This model currently uses a hybrid approach that combines large eddy simulation, for description of fluid dynamics, and the transport of the PDF with a single step global kinetic for modeling the combustion. The incorporation of a detailed thermochemistry mechanism would allow a better description of combustion, at the expense of a significant increase in computation time, which is not negligible in the case of a LES models. In this context, ISAT could be a viable option that may be able to decrease to an acceptable level the simulation time.

Finally, it is worth stressing that this study conducted verification tests of ISAT algorithm and PMSR reactor model only. No validation attempt was developed due to the difficulty of obtaining experimental data for such a homogeneous reactor configuration. This validation could be performed if carefully designed direct numerical simulations were available, or in more challenging flow problems, for instance.

## 5. ACKNOWLEDGMENTS

The authors acknowledge the support awarded to this research from Brazilian Council for Scientific and Technological Development (CNPq), Foundation for Research Support in Rio de Janeiro State (FAPERJ) and Brazilian Combustion Network. This work was performed while the second author was a Visiting Professor, funded by the Brazilian Petroleum Agency (ANP), on leave from Centre National de la Recherche Scientifique, France. The authors are indebted to Professor Guenther Carlos Krieger Filho from Universidade de São Paulo (USP), who provided the code that served as example to the code developed in this work, and for his hospitality during the authors visit to USP.

## 6. REFERENCES

Andrade, F. O. (2009). *Contribuition to the Lardy Eddy Simulation of a Turbulent Premixed Flame Stabilized in a High Speed Flow.* Doctoral Thesis, Pontifícia Universidade Católica do Rio de Janeiro, Rio de Janeiro. (in Portuguese).

Andrade, F. O., Figueira da Silva, L. F., and Mura, A. (2009). A Hybrid LES/SGS-PDF Computational Model for Turbulent Premixed Combustion. In *Proceedings of COBEM 2009.*

Correa, S. M. (1993). Turbulence-chemistry interactions in the intermediate regime of premixed combustion. *Combustion and Flame*, Vol. 93, No. 1-2, pp. 41–60. doi:10.1016/0010-2180(93)90083-F.

Cunha Jr, A. B. (2010). Reduction of Complexity in Combustion Thermochemistry. M.Sc. Dissertation, Pontifícia Universidade Católica do Rio de Janeiro, Rio de Janeiro.

Fox, R. O. (2003). *Computational Models for Turbulent Reacting Flows.* Cambridge University Press, Cambridge.

Gardiner, W. C. (2000). *Gas Phase Combustion Chemistry.* Springer, Ney York.

Golub, G. H. and Van Loan, C. F. (1996). *Matrix Computations.* John Hopkins University Press, Baltimore, 3rd edition.

Knuth, D. E. (1998). *The Art of Computer Programming, Volume 3: Sorting and Searching.* Addison-Wesley Professional, Boston, 2nd edition.

Pope, S. B. (1985). PDF methods for turbulent reactive flows. *Progress in Energy and Combustion Science*, Vol. 11, No. 2, pp. 119–192. doi:10.1016/0360-1285(85)90002-4.

Pope, S. B. (1997). Computationally efficient implementation of combustion chemistry using *in situ* adaptive tabulation. *Combustion Theory and Modelling*, Vol. 1, No. 1, pp. 41–63. doi:10.1080/713665229.

Pope, S. B. (2008). Algorithms for Ellipsoids. Technical Report FDA-08-01, Cornell University, Ithaca.

Williams, F. A. (1985). *Combustion Theory: the fundamental theory of chemically reacting flow systems.* Wesley, Cambridge, 2nd edition.

Yang, B. and Pope, S. B. (1998). An investigation of the accuracy of manifold methods and splitting schemes in the computational implementation of combustion chemistry. *Combustion and Flame*, Vol. 112, No. 1-2, pp. 16–32. doi:10.1016/S0010-2180(97)81754-3.